von Rad, U., Haq, B. U., et al., 1992
Proceedings of the Ocean Drilling Program, Scientific Results, Vol. 122

45. IRIDIUM AND OTHER ELEMENT DISTRIBUTIONS, MINERALOGY, AND MAGNETOSTRATIGRAPHY NEAR THE CRETACEOUS/TERTIARY BOUNDARY IN HOLE 761C[1]

Robert Rocchia,[2] Daniel Boclet,[3] Philippe Bonté,[2] Laurence Froget,[2] Bruno Galbrun,[4] Célestine Jéhanno,[2] and Eric Robin[2]

ABSTRACT

Samples from Ocean Drilling Program Hole 761C, collected on both sides of the Cretaceous/Tertiary boundary have been analyzed for their chemical and mineralogical content. The sediment consists of nannofossil ooze with variable amounts of clay. The boundary is marked by a color change associated with a nearly step-like decrease of the carbonate fraction. Paleomagnetic data and the drop of the carbonate content indicate that a strong reduction of the sedimentation rate occurred at the boundary and persisted for million of years. An iridium anomaly of 80 ng/cm^2, together with overabundances of Cr and Fe, are found in close coincidence with the planktonic crisis. These enrichments can be explained by the infall of =0.16 g/cm^2 of Cl-like chondritic material. Co and Ni enrichments and a great quantity of Ni-rich magnetites are also observed in the basal Danian. These elements and minerals excepted, the composition of the insoluble fraction appears to be nearly unchanged across the boundary. Chemical and mineralogical observations support a cosmic origin for the Cretaceous/Tertiary event but do not reveal the presence of any significant impact ejecta.

INTRODUCTION

Since the discovery by Alvarez et al. (1980) of an overabundance of iridium commonly attributed to a cosmic event, the number of sections exhibiting the same anomaly has increased to nearly 100. Although most complete sections systematically show a platinum group element abundance anomaly, they usually differ from one another because of local sedimentation conditions. Many marine Cretaceous/Tertiary (K/T) sites, especially those located in western Europe, were formed in a hemipelagic or a neritic environment and, therefore, were strongly influenced by the proximity of continents. The study of the boundary sequence at sites that formed under different depositional conditions is a good way to better understand the influence of the various sedimentary sources. Leg 122 offers the opportunity to explore an area where few K/T boundaries have been found so far. Hole 761C was cored on the Wombat Plateau, the most northern extension of the Exmouth Plateau, northeast of Australia. A complete core across the K/T boundary was recovered from a sedimentary sequence containing little terrigenous material that was formed in a pelagic environment (Haq, von Rad, O'Connell, et al., 1990). The Maestrichtian part of the core consists of white ooze of nannofossils; the Danian portion is richer in clay. There is no distinct clay layer at the boundary (see core photograph in Haq, von Rad, O'Connell, et al., 1990), which is marked by only a slight color change from white to light brown and green. This paper reports on the Ir enrichment at the K/T boundary in Hole 761C. It also includes discussions of paleomagnetic measurements across the boundary and preliminary results of our search for debris and other traces of cosmic origin.

ANALYTICAL METHODS

Sampling

Samples were provided in two sets. The first one continuously covers the interval between Sample 122-761C-3R-3, 52–53 cm, and Sample 122-761C-3R-3, 71–72 cm, with a 1-cm spacing. It was supposed to include the K/T boundary which, according to the study of calcareous nannofossils populations, was placed around interval 122-761C-3R-3, 67–68 cm. The rest of the section was more loosely sampled with a 5-cm step. Analyses of this first set of samples shows that the Ir maximum concentration is actually located between Sample 122-761C-3R-3, 71–72 cm, and Sample 122-761C-3R-3, 80–81 cm, well below the expected position. Then, additional samples taken in a 10-cm-long subcore covering the interval 122-761C-3R-3, 70–80 cm, were analyzed. The relative position of the two sets of samples was controlled thanks to the sharp color change observable in this subcore and in Sample 122-761C-3R-3, 75–76 cm. In view of the Ir distribution, which extends beyond the limits of the sampled interval, additional distant samples, some of them first used for paleomagnetic studies, were included in our routine for background determination.

Iridium and Other Elements

Elemental analyses were carried out by instrumental neutron activation analysis (INAA) of whole-rock samples. About 100 mg of ground and well-homogenized sample were dried, then sealed in a pure quartz vial. They were irradiated for a few hours in the 2×10^{14} n/cm^2/s neutron beam of the Osiris reactor at the Pierre Süe Laboratory, Saclay. Calibration standards are a piece of aluminium loaded with 5 ppm of Ir and USGS MAG1 for other elements. Iridium was counted with a γ-γ spectrometer detecting, without Compton rejection device, the 316–468 keV γ-ray coincidence resulting from the decay of ^{192}Ir. The sensitivity is such that concentrations as low as 50 picograms per gram (pg/g) can be significantly measured (3 standard deviation confidence level) after a 1-day accumulation time. Such good accuracy partly results from the improved performance of the γ-γ spectrometer over usual devices and partly from the low clay content of most samples.

[1] von Rad, U., Haq, B. U., et al., 1992. *Proc. ODP, Sci. Results*, 122: College Station, TX (Ocean Drilling Program).

[2] Centre des Faibles Radioactivités, Laboratoire Mixte CEA-CNRS, Avenue de la Terrasse, 91198 Gif-sur-Yvette Cedex, France.
[3] Service d'Astrophysique, CEN Saclay, 91191 Gif-sur-Yvette Cedex, France.
[4] Université de Paris VI, Département de Géologie Sédimentaire, URA CNRS 1314, 4 place Jussieu, 75252 Paris Cedex, France.

In order to determine Ir backgrounds as precisely as possible, several distant samples (more than 1 m away from the boundary) were counted together over a weekend. This permitted us to lower the sensitivity by a factor of 3 to 5. Concentrations of other elements were measured with a single high-purity Ge detector.

Paleomagnetism

Minicores oriented with respect to the upcore direction were drilled perpendicular to the axis of the split core at various depth intervals. Nine samples were taken in Core 122-761C-2R and 16 in Core 122-761C-3R. All the measurements were made with the 3-axis RS-01 (LETI/CEA) cryogenic magnetometer of the Département de Géologie Sédimentaire, Université Paris VI. The sensitivity of the instrument is such that it is possible to determine magnetization directions for samples with natural remanent magnetization (NRM) intensity as weak as 2×10^{-5} A/m with a good precision. Usual alternating field (AF) and thermal demagnetization techniques were used to isolate primary remanence components. The characteristic remanent magnetization (ChRM) directions were computed by applying the three-dimensional least-square line fit method of Kirschvink (1980).

Mineralogy

The determination of the mineral components was made by means of X-ray powder diffraction technique using a Philips goniometer equipped with a copper anode tube. Analyses were carried out on whole-rock powdered samples and some on the insoluble residues after dissolution of the carbonate fraction with 0.1-N acetic acid. We also measured major and minor element concentrations on compacted pellets with a LINK X-ray energy dispersive spectrometer (EDS) attached to a JEOL scanning electron microscope (SEM). Magnetically separated particles were analyzed with the SEM-EDS device.

The carbonate fraction was estimated from the Ca content measured both by INAA and EDS analysis. On a few samples, the process was checked by weighing the residue after carbonate dissolution.

RESULTS

Iridium and Other Siderophile Elements

The Ir abundance distribution is plotted in Figure 1 as a function of sample depth measured in meters below seafloor (mbsf). It is characterized by a sharp increase of the concentration in Sample 122-761C-3R-3, 75–76 cm (172.46 mbsf), in close coincidence with the color change observed at this level. The concentration remains nearly constant over a plateau of a few centimeters, followed by a tail extending over several tens of centimeters. Besides this major peak and two small bumps in the upward-extending tail, there is no outstanding sharp feature in the distribution. The main Ir anomaly is superimposed on a sort of shoulder that extends symmetrically on both sides of the boundary over a total thickness of 2 m of core. Estimates of the background concentrations, derived from the counting of most distant samples, have only a marginal statistical significance: 5 ± 2 (1-σ) pg/g for the Maestrichtian and 22 ± 8 (1-σ) pg/g during early Danian. To estimate the total mass of anomalous Ir at the K/T boundary we have integrated the Ir distribution multiplied by the average density ($d = 1.35$) over the interval of 2 m where the Ir concentration is significantly higher than the background. The total Ir flux is about 80 nanograms per square centimeter (ng/cm^2), representing a mass of 0.16 g/cm^2 of Cl-like chondritic material, if a meteoritic source is supposed. The shoulder represents about 40% of the total Ir infall.

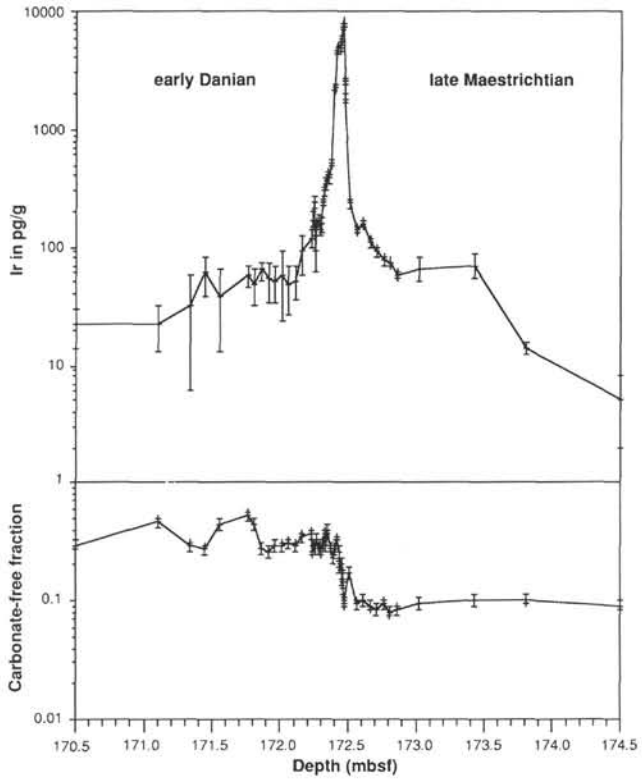

Figure 1. Distribution of Ir and carbonate-free fraction across the K/T boundary in Hole 761C. The Ir backgrounds in the Maestrichtian (175 to 177 mbsf) and in the Danian (170 to 171 mbsf) are 5 ± 2 pg/g and 22 ± 8 pg/g, respectively. Error bars are ± 1 standard deviation.

As far as other siderophile elements are concerned, Cr, Fe, Co, and Ni show significant excesses over their concentration in the terrigenous clay fraction. This is illustrated by the graphs in Figure 2 that display the abundances of these elements normalized to Sc. This element, as well as Th, is an excellent trace element indicator for the terrigenous clay component. The development of all these anomalies are rapid and somewhat shorter than the evolution of the Ir distribution. The excess of Sc-normalized abundances of Cr, Fe, Co, and Ni is determined in each sample by subtracting the terrigenous background level shown as dotted lines on Figure 2. The total elemental excess is then obtained by integrating the Sc-normalized excess values after multiplication by the Sc concentration, which varies from sample to sample. Doing that, we obtain an integrated Cr excess of 400 μg/cm^2 that can be explained by the fall of 0.15 g/cm^2 of Cl-like chondritic matter. A similar value of 0.14 g/cm^2 is derived from the integrated excess of Fe (26 mg/cm^2). Co and Ni, elements that are always associated with Ir in extraterrestrial matter, are not characterized by strong anomalies. The integrated excesses of Co (5.4 μg/cm^2) and Ni (65 μg/cm^2) are respectively consistent, with only 0.01 g/cm^2 and 0.006 g/cm^2 of Cl-like chondritic matter.

Rare-Earth Patterns and Other Elements

Whole-rock rare-earth element patterns (Fig. 3) normalized to chondrites are similar from the Maestrichtian (Fig. 3C) to the Danian (Fig. 3A) with no marked difference at the K/T boundary (Fig. 3B) defined as coinciding with the maximum Ir enrichment. The slight Ce depletion indicates that a small amount of rare-earth elements was derived from seawater. This anomaly is present all along the core with no detectable

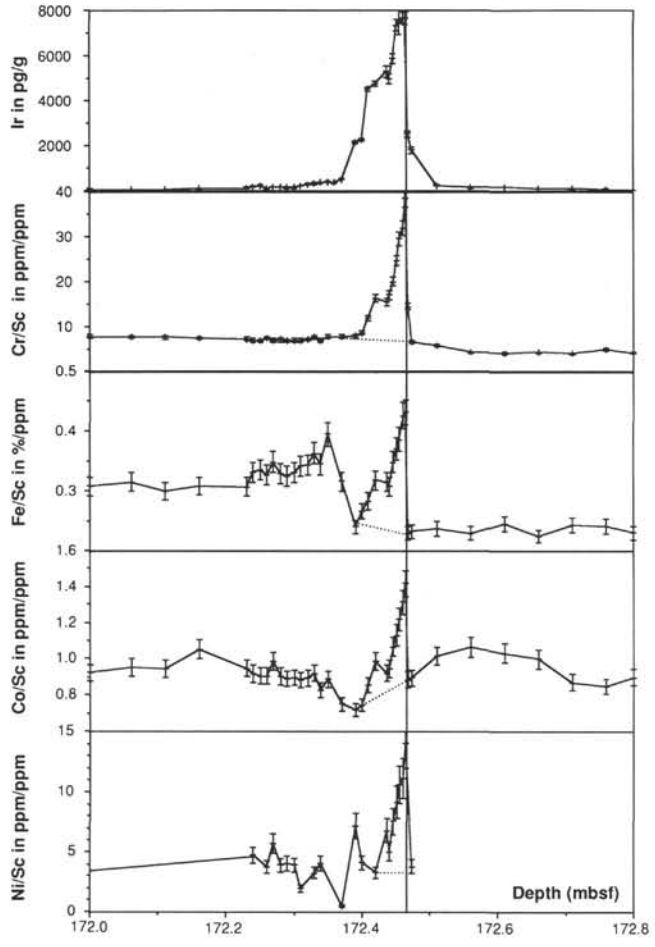

Figure 2. Distribution of Ir and Sc-normalized abundances of Cr, Fe, Co, and Ni vs. stratigraphic depth (mbsf). The distributions of Cr, Fe, Co, and Ni are well correlated and more narrow than the Ir anomaly.

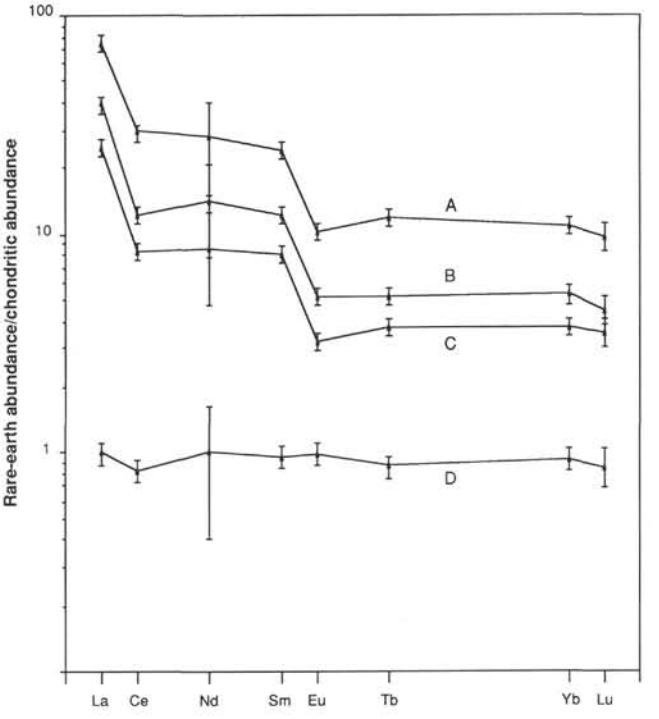

Figure 3. Rare-earth elements abundances normalized to chondrites as a function of atomic number. **A.** Danian, 20 cm above the boundary; Sample 122-761C-3R-3, 55–56 cm (172.26 mbsf). **B.** K/T boundary defined as the maximum of Ir enrichment; Sample 122-761C-3R-3, 75–76 cm (172.464 mbsf). **C.** Maestrichtian, 20 cm below the boundary; Sample 122-761C-3R-3, 95–96 cm (172.66 mbsf). **D.** (0.5 × boundary)/(Maestrichtian + Danian), normalized to lanthanum. Error bars are ±3 standard deviations.

change at the K/T boundary (Fig. 3D). However, the La/Yb ratio which is about 10:12 in the Maestrichtian, regularly increases from K/T boundary up to a maximum of 15 occurring 7–8 cm above it, and then returns to the initial value of 10:12 in the rest of the Danian.

Th, Cs, Hf, Ta, Sc, and Al (Table 1) all follow the evolution of the clay fraction.

Mineralogy

All whole-rock X-ray-diffraction spectra are dominated by calcite (Figs. 4A, 4B, 4C, and 5). Three other phases appear which are smectite and clinoptilolite with little quartz. In addition to these phases, some samples located near siliceous concretions contain abundant opal-CT. We note that the same mineralogic phases are continuously observed from the Cretaceous to the Paleocene with no change at the K/T boundary (compare spectrum in Fig. 4B with 4A and 4C). Clinoptilolite (Pl. 1A and 1B) and smectite are authigenic phases that likely arise from the alteration of volcanic glasses. We have no reason to suspect that, at the very K/T boundary, these minerals would have a different origin. Quartz is detrital whereas opal-CT has a biogenic origin. Spectra of X-ray diffraction carried out on the insoluble fraction only (Fig. 5) do not reveal other phases than those previously observed in whole-rock samples and show that smectite and clinoptilolite are fairly well crystallized.

Optical observations and magnetic extraction reveal the existence in the first few centimeters of the Danian of a great quantity of black Ni-rich magnetite crystals. These crystals are often clustered in flat pancakes or lenses (Pl. 1C), sometimes exceeding several hundred microns in diameter. These clusters are aligned parallel to the deposition plane and are analogous to flattened spheroids found in some other K/T sections and described by Montanari et al. (1983), Smit and Kyte (1984), and Kyte and Smit (1986). The typical composition of magnetites is 5%–10% Mg, 2%–4% Al, 0.5%–2% Cr, 50%–55% Fe, and 2%–6% Ni. Individual crystals are rather large: magnetites exceeding 10–15 μm are common (Pl. 1D). They are embedded in a matrix of clay which is possibly the result of alteration of some original material, probably spherical in shape, that was subsequently flattened during compaction.

A brief microscopic examination of Sample 122-761C-3R-3, 75–76 cm, did not reveal the presence of shocked quartz; however, its absence in this small sample (<1 g) does not preclude its possible discovery in later investigations of samples from Hole 761C.

Magnetostratigraphy

Alternating field (AF) and thermal demagnetization both produced good results. An unstable component was removed by heating at 100°C or by 5–10 mT AF demagnetization, and a stable component is observed within the 150°–400°C or 10–30 mT range of demagnetization steps (Fig. 6).

Since borehole cores are not azimuthally oriented, only inclination values are used for interpretation (Table 2). With the exception of two samples of normal polarity (122-761C-

Table 1. Elemental abundances across the K/T boundary in Hole 761C.

Core, section, interval (cm)	Depth (mbsf)	CaCO3	Sr ppm	Mg %	Al %	Si %	Fe %	Sc ppm	Th ppm	Hf ppm	Ta ppm	Cs ppm	Rb ppm	Ba ppm
122-761C-														
2R-2, 124-125	162.940	0.615	610	0.4	0.9	15.2	0.47	1.89	1.90	0.30	0.090	0.58	12	450
2R-3, 118-119	164.380	0.776	689	0.5	1.8	6.3	1.00	3.43	3.70	0.61	0.180	1.30	21	430
3R-1, 48-49	170.180	0.689		1.0	2.6	9.0								
3R-1, 63-64	170.330	0.697		0.7	2.3	9.4								
3R-1, 102-103	170.720	0.702		0.9	2.2	8.3								
3R-1, 140-141	171.100	0.532		0.5	2.1	17.3								
3R-2, 14-15	171.340	0.712		0.7	2.2	8.4								
3R-2, 25-26	171.450	0.727		0.7	2.7	7.4								
3R-2, 35-36	171.550	0.550		1.1	4.8	11.9								
3R-2, 48-49	171.680	0.561	604	1.0	3.4	12.8	1.90	7.13	6.80	1.30	0.360	3.10	45	1730
3R-3, 5-6	171.760	0.473	550	1.1	4.0	16.1	2.13	6.95	7.00	1.30	0.350	3.00	42	1340
3R-3, 10-11	171.810	0.556	526	0.9	3.4	13.5	1.93	6.88	7.00	1.30	0.400	3.00	45	1000
3R-3, 15-16	171.860	0.723	665	0.6	1.9	8.2	1.59	4.93	5.00	1.00	0.270	2.00	34	1080
3R-3, 20-21	171.910	0.739	672	0.6	1.9	7.5	1.22	3.82	3.60	0.76	0.220	1.50	23	1100
3R-3, 25-26	171.960	0.706	568	0.7	2.2	8.7	1.56	5.10	5.00	1.10	0.300	2.20	33	1510
3R-3, 30-31	172.010	0.710	632	0.6	2.1	8.5	1.40	4.55	4.40	0.90	0.250	1.90	28	1120
3R-3, 35-36	172.060	0.694	623	0.7	2.2	9.0	1.42	4.51	4.40	0.90	0.250	1.90	35	1080
3R-3, 40-41	172.110	0.711	732	0.6	2.2	8.7	1.17	3.90	3.70	0.70	0.220	1.50	27	1160
3R-3, 45-46	172.160	0.658	714	0.8	2.5	9.7	1.52	4.93	4.80	1.00	0.310	1.90	39	1130
3R-3, 52-53	172.230	0.634	750	0.8	2.8	11.0	1.77	5.76	5.40	1.20	0.290	2.20	37	1450
3R-3, 53-54	172.240	0.732	616	0.7	2.0	7.6	1.75	5.27	4.70	0.80	0.200	1.60	27	950
3R-3, 54-55	172.250	0.711	574	0.8	2.2	8.0	1.85	5.52	4.70	0.85	0.180	1.70	26	1070
3R-3, 55-56	172.260	0.727	634	0.8	1.9	7.6	1.75	5.35	4.70	0.85	0.180	1.60	25	1070
3R-3, 56-57	172.270	0.668	572	0.7	2.1	8.0	1.83	5.25	5.10	0.90	0.230	1.70	30	1100
3R-3, 57-58	172.280	0.726	600	0.7	2.1	8.0	1.67	5.08	4.40	0.80	0.200	1.50	26	1110
3R-3, 58-59	172.290	0.700	593	0.8	2.3	8.5	1.75	5.38	4.70	0.80	0.190	1.70	27	1020
3R-3, 59-60	172.300	0.732	566	0.7	2.0	7.7	1.70	5.12	4.50	0.80	0.180	1.60	28	1020
3R-3, 60-61	172.310	0.691	523	0.9	2.4	8.6	1.70	4.97	4.60	0.70	0.200	1.60	27	960
3R-3, 61-62	172.320	0.703	587	0.8	2.4	8.5	1.82	5.30	4.70	0.70	0.180	1.70	28	940
3R-3, 62-63	172.330	0.633	527	0.9	2.6	10.3	2.33	6.41	6.10	1.00	0.260	2.20	34	1150
3R-3, 63-64	172.340	0.707	536	0.8	2.0	8.2	1.95	5.65	4.80	0.90	0.200	1.80	28	1240
3R-3, 64-65	172.350	0.596	495	1.0	3.0	11.6	2.60	6.58	6.40	1.10	0.250	2.30	35	1520
3R-3, 66-67	172.370	0.716	520	0.8	2.0	7.9	1.77	5.60	5.20	1.00	0.190	1.90	32	1490
3R-3, 68-69	172.390	0.768	675	0.5	1.7	7.0	0.94	3.90	3.58	0.72	0.190	1.60	26	280
3R-3, 69-70	172.400	0.726	795	0.6	2.1	8.2	1.36	5.10	5.10	1.00	0.260	2.00	37	370
3R-3, 70-71	172.410	0.699	718				1.06	3.74	3.60	0.68	0.180	1.50		340
3R-3, 71-72	172.420	0.679	844	1.0	2.2	9.2	1.16	3.65	3.40	0.65	0.180	1.30	21	265
3R-3, 72.5-72.8	172.431	0.736	749	0.6	2.0	7.6	1.05	3.33	2.98	0.60	0.166	1.06	20	277
3R-3, 73.0-73.3	172.436	0.780	694	0.5	1.6	5.8	0.91	2.97	2.38	0.51	0.135	0.88	18	223
3R-3, 73.5-73.8	172.441	0.791	783	0.6	1.5	5.9	1.07	3.07	2.61	0.53	0.142	0.93	18	284
3R-3, 74.0-74.3	172.446	0.826	851	0.5	1.2	4.8	1.02	2.75	2.19	0.46	0.116	0.76	14	293
3R-3, 74.5-74.8	172.451	0.846	880	0.5	1.1	4.2	0.94	2.43	1.91	0.39	0.096	0.63	12	352
3R-3, 75.0-75.3	172.456		803				0.96	2.31	1.81	0.41	0.101	0.62	10	301
3R-3, 75.3-75.5	172.459	0.870	847	0.4	0.9	3.6	0.93	2.16	1.72	0.35	0.098	0.57	11	334
3R-3, 75.5-75.8	172.461	0.850	906	0.4	1.0	3.9	0.88	2.05	1.73	0.33	0.091	0.54	11	351
3R-3, 75.8-76.0	172.464	0.902	926				0.48	1.57	1.02	0.21	0.056	0.34	6	482
3R-3, 76-76.3	172.466	0.900	997				0.36	1.49	0.96	0.19	0.049	0.31	7	471
3R-3, 76.3-76.5	172.469		963				0.35	1.46	1.01	0.19	0.048	0.32	6	446
3R-3, 80-81	172.510	0.828	995	0.2	0.5	6.5	0.28	1.18	1.10	0.20	0.050	0.35	7	410
3R-3, 85-86	172.560	0.906	1170	0.2	0.4	2.8	0.28	1.22	1.10	0.20	0.060	0.40	5	495
3R-3, 90-91	172.610	0.898	1193	0.3	0.5	3.1	0.31	1.26	1.15	0.23	0.050	0.40	5	480
3R-3, 95-96	172.660	0.908	1140	0.3	0.5	2.4	0.27	1.20	1.10	0.20	0.050	0.40	5	485
3R-3, 100-101	172.710	0.915	1071	0.2	0.5	2.3	0.31	1.27	1.15	0.23	0.052	0.35	7	480
3R-3, 105-106	172.760	0.907	1137	0.2	0.6	2.5	0.34	1.43	1.30	0.20	0.060	0.40	8	450
3R-3, 110-111	172.810	0.918	874	0.3	0.5	2.0	0.23	1.01	0.90	0.16	0.040	0.31		380
3R-3, 115-116	172.860	0.917	1012	0.3	0.5	2.0	0.28	1.19	1.10	0.18	0.050	0.38	6	420
3R-3, 130-131	173.020	0.905		0.2	0.6	2.2								
3R-4, 21-22	173.430	0.898		0.2	0.6	2.6								
3R-4, 59-60	173.810	0.897	1146	0.4	0.6	2.6	0.31	1.27	1.10	0.23	0.050	0.38	7	460
3R-4, 80-81	174.020	0.911		0.3	0.5	2.2								
3R-4, 121-123	174.430	0.908		0.3	0.6	2.2								
3R-5, 30-31	175.020	0.924		0.3	0.4	1.5								
3R-5, 45-46	175.170	0.929	1072	0.2	0.4	1.7	0.24	1.15	0.90	0.20	0.040	0.33	6	520
3R-5, 107-108	175.790	0.907		0.2	0.6	2.2								
3R-6, 83-84	177.050	0.892	1127	0.4	0.8	2.7	0.45	1.88	1.60	0.30	0.060	0.45	8	670

Note: 1-σ uncertainties are 1%–3% for Fe, Sc, Th, Ce, Cr, Co, Eu; 3%–5% for $CaCO_3$, Si, Sr, Cs, Zn, Hf, Tb, Yb, La, Sm; 5%–10% for Ba, Rb, Lu; and 10%–15% for Al, Mg, Ni, Nd.

2R-2, 20–22 cm, and 122-761C-2R-3, 70–72 cm), Core 122-761C-2R is mainly of reversed polarity. Core 122-761C-3R shows the following polarity sequence: reversed at the top, normal from 170.72 to 171.92 mbsf and reversed from 172.25 mbsf to the base of the core at 177.05 mbsf.

Comparison of this polarity pattern with the polarity time scale of Haq et al. (1987), aided by paleontological data (Haq, von Rad, O'Connell, et al., 1990), leads to the identification of Chrons 26 to 29 (Fig. 7). The lower part of Core 122-761C-3R corresponds to the reversed-polarity Chron 29R; the base of this chron was not cored at Hole 761C. The upper boundary of this chron with the normal-polarity Chron 29N occurs between Sample 122-761C-3R-3, 20–22 cm (171.92 mbsf), and Sample 122-761C-3R-3, 53–55 cm (172.25 mbsf). The boundary between Chron 29N and reversed-polarity Chron 28R occurs between Sample 122-761C-3R-1, 63–65 cm (170.33 mbsf), and Sample 122-761C-3R-1, 102–104 cm (170.72 mbsf). In the absence of a base for Core 122-761C-2R, the correlation of the polarity sequence of this core with the polarity reference time scale is less straightforward. However, biozonation shows that it is likely to correspond with the upper part of the reversed-polarity Chron 27R and Chron 26.

Sedimentation Rate

Sedimentation rates are derived from the positions of the top and base of Chron 29. According to Haq et al. (1988), the top of Chron 29N occurs at 64.91 Ma and the base of Chron 29R at 66.96 Ma, the K/T boundary itself being at 66.5 Ma.

Table 1 (continued).

Zn ppm	La ppm	Ce ppm	Nd ppm	Sm ppm	Eu ppm	Tb ppm	Yb ppm	Lu ppm	Cr ppm	Co ppm	Ni ppm	Ir ppb
19	9.0	8.0	7.0	1.90	0.32	0.22	0.75	0.12	11.0	1.58		
35	12.5	13.9	10.7	2.60	0.46	0.33	1.00	0.16	25.0	3.15	12.0	
												0.022 ± 0.008
												0.022 ± 0.009
												0.032 ± 0.026
												0.061 ± 0.022
												0.038 ± 0.025
64	24.0	31.0	18.0	4.90	0.85	0.70	2.20	0.34	54.0	5.20	23.0	
69	25.0	33.0	19.4	5.20	0.85	0.70	2.20	0.41	57.0	5.64	22.0	0.058 ± 0.012
60	24.0	31.0	17.0	5.20	0.80	0.60	2.10	0.42	56.0	5.10		0.049 ± 0.017
47	20.0	23.4	16.0	4.50	0.66	0.50	1.85	0.29	39.0	4.35	17.0	0.063 ± 0.011
38	13.0	18.0	13.2	2.90	0.59	0.42	1.40	0.24	30.0	3.69		0.053 ± 0.020
51	22.0	22.0	15.0	5.50	0.77	0.57	1.80	0.31	38.0	4.50		0.051 ± 0.018
48	18.0	20.4	14.0	4.30	0.67	0.50	1.50	0.27	36.0	4.20		0.058 ± 0.035
48	17.0	20.0	14.0	3.90	0.67	0.50	1.50	0.24	35.0	4.30		0.047 ± 0.020
42	16.0	18.0	13.0	3.60	0.60	0.48	1.46	0.24	30.0	3.70		0.052 ± 0.016
44	19.0	22.0	16.7	4.50	0.70	0.60	1.80	0.26	37.0	5.20		0.091 ± 0.035
54	20.0	22.0	14.0	4.60	0.74	0.55	1.70	0.30	42.0	5.47		0.120 ± 0.020
54	23.0	22.0	14.0	4.40	0.73	0.60	2.00	0.34	37.0	4.85	25.0	0.171 ± 0.024
62	23.0	24.0	17.0	4.30	0.76	0.60	2.00		38.0	5.00		0.244 ± 0.026
58	24.0	23.0	16.0	4.50	0.73	0.60	2.00	0.33	40.0	4.85	20.0	0.094 ± 0.033
57	22.0	23.0	16.0	4.50	0.71	0.57	1.90	0.29	37.0	5.20	30.0	0.156 ± 0.007
65	23.0	22.0	15.0	4.20	0.70	0.60	2.10	0.28	36.0	4.60	20.0	0.171 ± 0.014
61	24.0	23.0	17.0	4.60	0.74	0.57	2.00	0.35	37.0	4.80	22.0	0.139 ± 0.014
55	22.0	22.0	15.3	4.20	0.67	0.60	1.90	0.32	36.0	4.60	20.0	0.156 ± 0.022
57	24.0	21.4	17.0	4.60	0.70	0.55	2.00	0.35	35.0	4.40	10.0	0.234 ± 0.015
56	25.0	22.0	18.2	4.70	0.72	0.55	1.95	0.32	38.0	4.75		0.297 ± 0.021
67	27.0	28.0	20.6	5.20	0.92	0.72	2.20	0.35	49.0	5.90	21.0	0.342 ± 0.041
62	25.0	24.5	17.8	4.60	0.82	0.70	2.20	0.33	40.0	4.70	23.0	0.363 ± 0.023
79	29.0	30.0	20.5	5.70	1.00	0.80	2.30	0.34	52.0	5.85		0.405 ± 0.027
56	32.0	25.6	23.0	6.10	0.88	0.70	2.20	0.37	44.0	4.20	3.0	0.518 ± 0.029
38	20.0	16.0	15.4	4.30	0.60	0.47	1.38	0.26	31.0	2.80	28.0	2.153 ± 0.042
57	21.0	21.5	20.0	4.70	0.80	0.60	1.60	0.26	44.0	3.80	21.0	2.289 ± 0.055
38		15.5	13.0		0.69	0.46	1.15		45.0	3.20		4.543 ± 0.076
38	18.0	14.0	14.6	3.70	0.61	0.41	1.20	0.18	60.0	3.60	12.0	4.777 ± 0.133
39	18.0	14.0	14.3	3.62	0.59	0.41	1.25	0.18	53.5	3.07	22.7	5.333 ± 0.250
57	16.3	11.4	12.5	2.93	0.48	0.32	1.05	0.17	50.4	2.81	15.0	4.990 ± 0.240
32	16.1	12.5	12.9	3.05	0.51	0.37	1.13	0.17	65.3	3.28	23.2	5.912 ± 0.220
29	14.3	11.4	10.8	2.54	0.45	0.31	1.01	0.15	76.0	3.11	25.2	7.356 ± 0.270
26	13.4	10.5	12.8	2.34	0.41	0.28	1.02	0.16	76.4	2.96	25.8	7.490 ± 0.520
50	13.3	9.6	9.1	2.51	0.40	0.29	0.94	0.15	79.3	3.05	27.6	7.680 ± 0.240
28	12.7	9.4	8.2	2.15	0.37	0.27	0.92	0.15	86.6	2.97	27.9	7.663 ± 0.250
25	12.5	9.6	8.4	2.15	0.38	0.28	0.97	0.15	83.3	2.98	31.3	7.622 ± 0.310
14	10.9	6.3	6.1	1.58	0.26	0.20	0.92	0.15	30.5	1.54	10.9	2.866 ± 0.130
16	9.5	6.4	5.9	1.45	0.24	0.20	0.95	0.14	13.5	1.32	7.1	2.212 ± 0.150
15	9.8	6.2	5.9	1.44	0.25	0.20	0.90	0.14	10.3	1.35	5.5	1.810 ± 0.150
12	8.0	6.5	5.0	1.40	0.22	0.18	0.70	0.13	6.8	1.20		0.235 ± 0.018
18	8.0	6.7	5.0	1.40	0.24	0.19	0.80	0.11	5.3	1.30		0.141 ± 0.009
16	9.0	6.7	5.5	1.50	0.24	0.20	0.70	0.14	5.3	1.30		0.156 ± 0.010
14	8.0	6.6	5.0	1.50	0.23	0.19	0.70	0.12	5.2	1.20		0.109 ± 0.009
17	8.0	5.9	6.1	1.40	0.24	0.20	0.70	0.11	5.2	1.11		0.091 ± 0.008
17	7.0	5.0	8.0	1.90	0.25	0.20	0.70	0.09	7.0	1.20		0.077 ± 0.007
12		5.0	5.0		0.20	0.14	0.50		4.3	0.91		0.071 ± 0.004
16		6.2	5.9		0.25	0.17	0.63		5.3	1.08		0.058 ± 0.003
												0.066 ± 0.014
												0.070 ± 0.017
14	8.0	6.4	5.0	1.40	0.23	0.18	0.65	0.10	5.1	1.02		0.014 ± 0.002
												0.005 ± 0.003
12	8.0	6.2	4.0	1.50	0.24	0.21	0.70	0.13	4.2	1.15		
												0.004 ± 0.003
21	12.2	10.0	7.9	2.20	0.38	0.30	1.00	0.16	6.1	1.81		0.005 ± 0.002

The Maestrichtian part of Chron 29 (about 460 10^3 yr) extends over at least 4.58 m. The thickness of the Danian part of Chron 29 (about 1.59 10^6 yr) is between 1.75 m and 2.14 m. The average sedimentation rate is therefore higher than 10.4 m/m.y. in the Maestrichtian and between 1.1 and 1.3 m/m.y., at the base of the Danian, nearly 10 times lower. The data showing the carbonate and insoluble fraction deposition rates are displayed in Table 3.

Data from Core 122-761C-2R permit the evaluation of the sedimentation rate on a longer time scale. The top of Chron 27 (61.36 Ma) is around 164 mbsf, about 8–9 m above the boundary. The average sedimentation rate during most of the Danian can therefore be estimated at about 1.7 m/m.y., close to the value found for the basal Danian. This shows that the rate of deposition was rather low and stable for the few millions years following the K/T event, in agreement with the high and nearly constant insoluble fraction observed during that period.

DISCUSSION

The onset of the main Ir anomaly is very sharp and occurs in Sample 122-761C-3R-3, 75–76 cm, in a part of the core which seems to be free of coring disturbance (see core picture in Haq, von Rad, O'Connell, et al., 1990). The presence of siliceous nodules around Sections 122-761C-3R-3, 65 cm, and 122-761C-3R-3, 80 cm, could have locally damaged the quality of the core but has not produced any visible feature in the Ir distribution. The difference in position between the Ir-defined

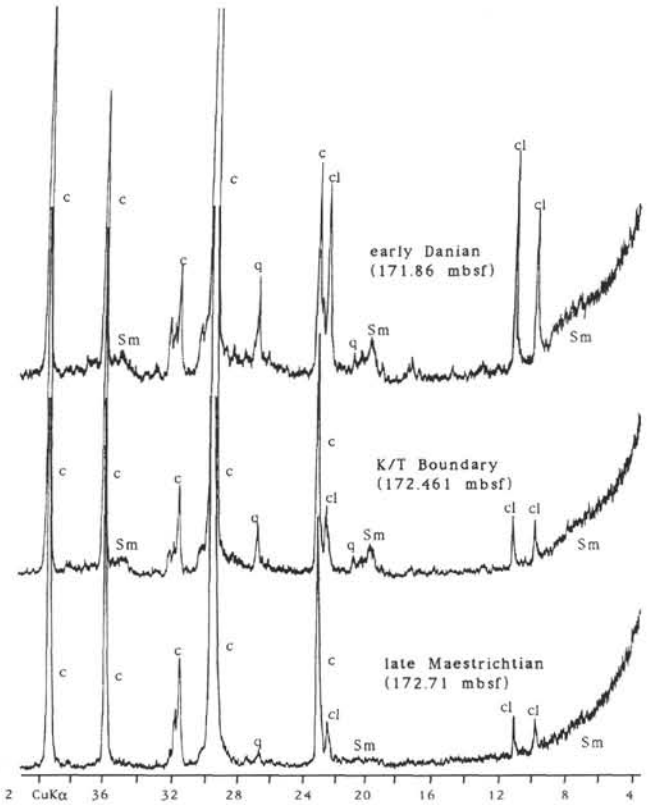

Figure 4. Diffraction spectra of whole-rock samples showing calcite (c), clinoptilolite (cl), quartz (q), and smectite (Sm) lines. No change of the mineralogical components occurs across the boundary.

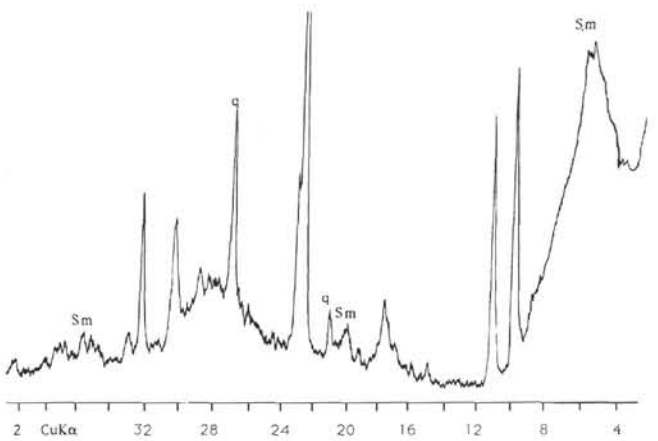

Figure 5. Typical diffraction spectrum of a decarbonated sample. All samples display similar spectrum showing well-crystallized phases. Only smectite (Sm) and quartz (q) lines are noted; others are those of clinoptilolite.

boundary (Sample 122-761C-3R-3, 75–76 cm, 172.46 mbsf) and the biostratigraphic position (Sample 122-761C-3R-3, 67–68 cm, 172.38 mbsf; the base of Zone NP1) is essentially a matter of definition. As pointed out by Smit and Romein (1985), in all complete sections the nannofossil-defined K/T boundary (first occurrence of Tertiary nannofossils) is located above the mass extinction level which is systematically observed in coincidence with the rapid increase of the Ir concentration. So, the boundary, if defined by the mass extinction level or the Ir distribution, should be moved down by 8–9 cm with respect to the previously quoted position based on the first occurrence of Tertiary nannofossils (Haq, von Rad, O'Connell, et al., 1990).

The meaning of the low Ir excess that extends symmetrically on both sides of the main anomaly is not clear. Officer and Drake (1985) showed that it cannot be explained by the bioturbation of a quasi-instantaneous event. Does it mean that the Ir distribution represents a long duration event? Two types of scenarios involving multiple episodes have been proposed to explain the K/T boundary features. Hut et al. (1987) propose that multiple collisions of comets explain the stepwise precursory biological extinctions (Keller, 1989) occurring at the end of the Maestrichtian. Officer and Drake (1983) and Courtillot and Cisowski (1987) postulate the existence of a period of intense volcanic activity associated with the Deccan traps formation. In this paper, without entering into the debate, we can, however, note that the Ir distribution curve is rather smooth and does not indicate the occurrence of multiple discrete events. Comparison with other K/T sections provide useful information. At Hole 761C, the Ir anomaly, shoulder included, covers an interval of about 10^6 years, suggesting an event of long duration. However, in several European sections the Ir excess is also observed over about 1–2 m, which represents only 10^4–10^5 yr of deposition (Rocchia et al. 1987). This apparent inconsistency suggests that the full extent of the Ir anomaly does not represent the actual duration of the K/T event. It is more likely due to postdepositional geochemical processes.

The magnetostratigraphic study of Cores 122-761C-2R and 122-761C-3R has permitted the identification of the magnetic polarity sequence near the K/T boundary and a reasonably accurate estimate of the sedimentation rates in the late Maestrichtian and early Danian. The planktonic crisis reduced the carbonate deposition rate by a factor of 10. The sedimentation rate of the insoluble fraction also suffered a smaller but still important reduction by a factor of 3 to 4. This is a surprising but not new fact; it has already been observed in many K/T sections (Zachos et al., 1985; Rocchia et al., 1987; Timothy and D'Hondt, 1990). This reduction of the insoluble-fraction deposition rate is not a local feature but appears to be global. Until now, it has not been convincingly explained. Indeed, it is easy to understand that the planktonic turnover at the boundary could significantly change the carbonate production. That it could also reduce the deposition rate of the nonbiogenic component is not obvious at all. It implies that the machinery of sediment production and transportation has been disturbed on a global scale for millions of years.

With the deposition rates derived from magnetostratigraphy, we can check the consistency of our Ir background estimates with the value of the steady-state Ir infall. As pointed out above, our measurements are not really statistically significant and they permit us only to derive upper limits. With a 3-σ criterion we can say that Ir concentrations are lower than 10 pg/g for the Maestrichtian and 45 pg/g for the Danian. According to Kyte and Wasson (1986), the steady-state extraterrestrial Ir flux is 9 ng/cm^2/m.y. We have not included in that budget the terrestrial contribution, which can change from one site to the other. Assuming constant sedimentation rates below (>10 m/m.y.) and above the K/T boundary (1.6 m/m.y. between the K/T boundary and top of Chron 27), the Ir concentration should be lower than 6 pg/g during the Maestrichtian part of Chron 29R and about 45 pg/g up to the top of Core 122-761C-2R. Taking into account the large uncertainties of our measurements and of the Kyte and Wasson budget, we can conclude that they are consistent with each other for the Maestrichtian and for the Danian as well. It is

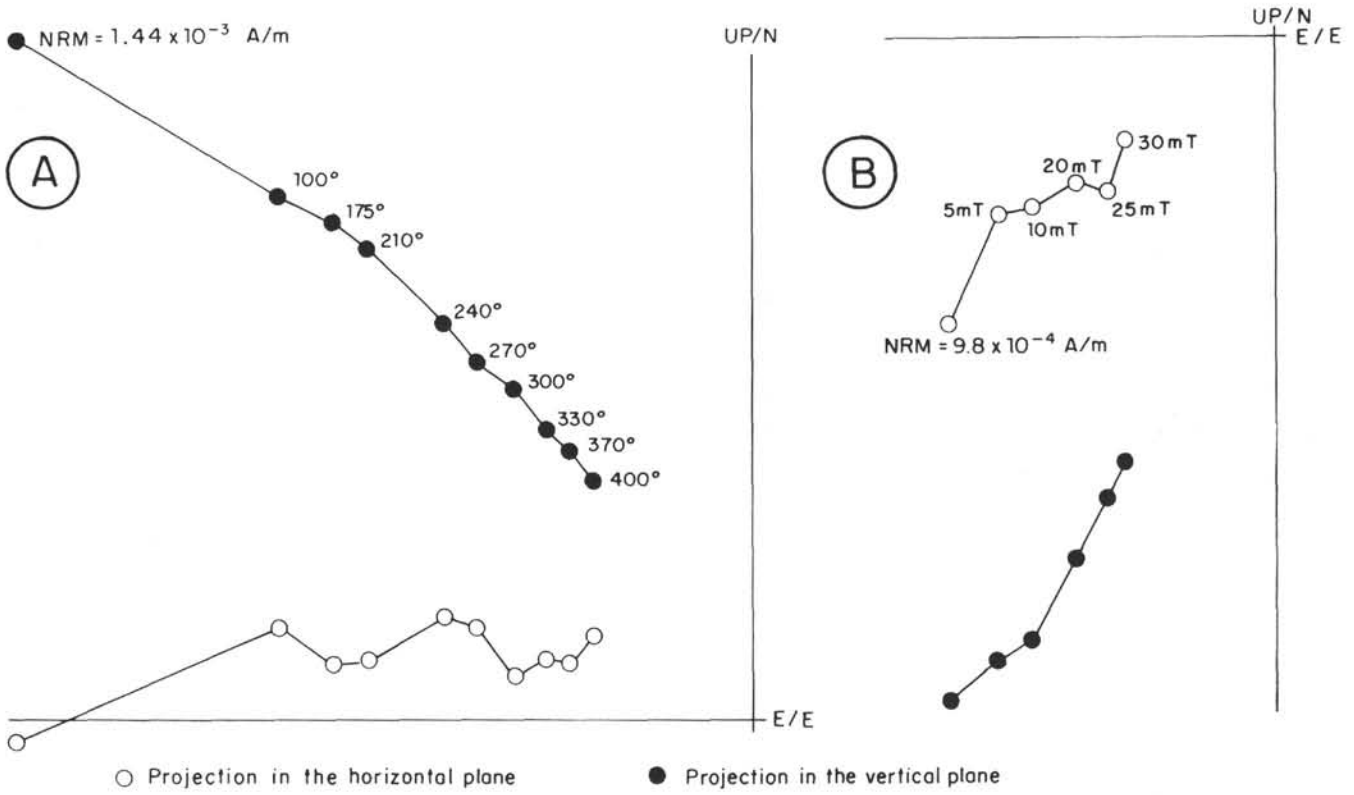

Figure 6. Orthogonal vector plots of demagnetization curves for two samples illustrating typical magnetic behaviors. **A.** Thermal demagnetization, Sample 122-761C-2R-2, 20–22 cm. **B.** AF demagnetization, Sample 122-761C-2R-2, 124–126 cm. An initial unstable component is removed by 100°C heating or by 5–10 mT AF demagnetization. Above those values the ChRM directions are defined and are of normal (A) or reversed (B) polarity.

Table 2. Direction of characteristic magnetization, K/T boundary (Cores 122-761C-2R and -3R).

Core, section, interval (cm)	Depth (mbsf)	NRM (A/m)	Inclination (°)	Demagnetization step
122-761C-				
2R-1, 102	161.22	3.91 E-3	+24	30 mT
2R-2, 20	161.90	1.44 E-3	−51	400°C
2R-2, 71	162.41	7.50 E-5	+70	370°C
2R-2, 124	162.94	9.82 E-4	+50	30 mT
2R-3, 20	163.40	8.10 E-5	+57	400°C
2R-3, 70	163.90	2.19 E-4	−50	400°C
2R-3, 118	164.38	2.80 E-5	+69	30 mT
2R-3, 140	164.60	5.50 E-5	+54	400°C
2R-4, 51	165.21	4.10 E-5	+72	30 mT
3R-1, 48	170.18	5.60 E-5	+54	400°C
3R-1, 63	170.33	4.70 E-5	+60	30 mT
3R-1, 102	170.72	5.00 E-5	−44	300°C
3R-1, 140	171.10	1.09 E-4	−50	370°C
3R-2, 14	171.34	6.50 E-5	−26	330°C
3R-2, 48	171.68	1.15 E-4	−37	30 mT
3R-3, 20	171.92	1.01 E-4	−48	300°C
3R-3, 53	172.25	9.70 E-5	+45	270°C
3R-3, 112	172.84	1.08 E-4	+24	30 mT
3R-4, 21	173.43	1.70 E-4	+29	400°C
3R-4, 59	173.81	8.00 E-5	+50	30 mT
3R-4, 121	174.43	1.02 E-4	+55	400°C
3R-5, 45	175.17	5.30 E-5	+62	30 mT
3R-5, 107	175.79	1.95 E-4	+53	400°C
3R-6, 18	176.40	8.30 E-5	+62	30 mT
3R-6, 83	177.05	9.10 E-5	+67	400°C

important to note that the Danian background was measured in samples that are rather close to the upward-extending part of the Ir distribution. A different estimate could be obtained in more distant samples. Additional measurements up to the top of Core 122-761C-2R are required to corroborate that point.

As far as the nature of the K/T event is concerned, all observations point to a cosmic origin. The presence of Ir and its ratio in chondritic proportion with Cr and Fe strongly support a dramatic increase of the cosmic matter accretion rate at the K/T boundary. The significantly lower Ni enrichment is not inconsistent with this hypothesis. It is a common feature already observed in other K/T sites and could be due to dissolution of Ni oxide in seawater (Alvarez et al. 1980). The presence of Ni-rich magnetites often clustered in flattened spheroids provides the most convincing signature for an extraterrestrial origin. These minerals have no counterparts in terrestrial materials (Smit and Kyte, 1984; Kyte and Smit, 1986). Smaller crystals of this type are abundant in micrometeorites (Brownlee, 1981; Bonté et al., 1987; Robin et al., 1990) but, with their composition and size, magnetites from Hole 761C look more like those found in meteoritic ablation products from a Jurassic sequence from northern Italy (Jéhanno et al., 1987). In this Jurassic site, Ni-rich magnetites are locked in host bodies which, because of their perfectly preserved internal structures, can be unambiguously identified with cosmic particulates. Conversely, magnetites of the K/T boundary at Hole 761C are located in highly weathered, altered, and damaged bodies that cannot be immediately identified on purely morphological considerations. However, their chemical composition shows that they are likely to constitute the relics of pure meteoritic debris.

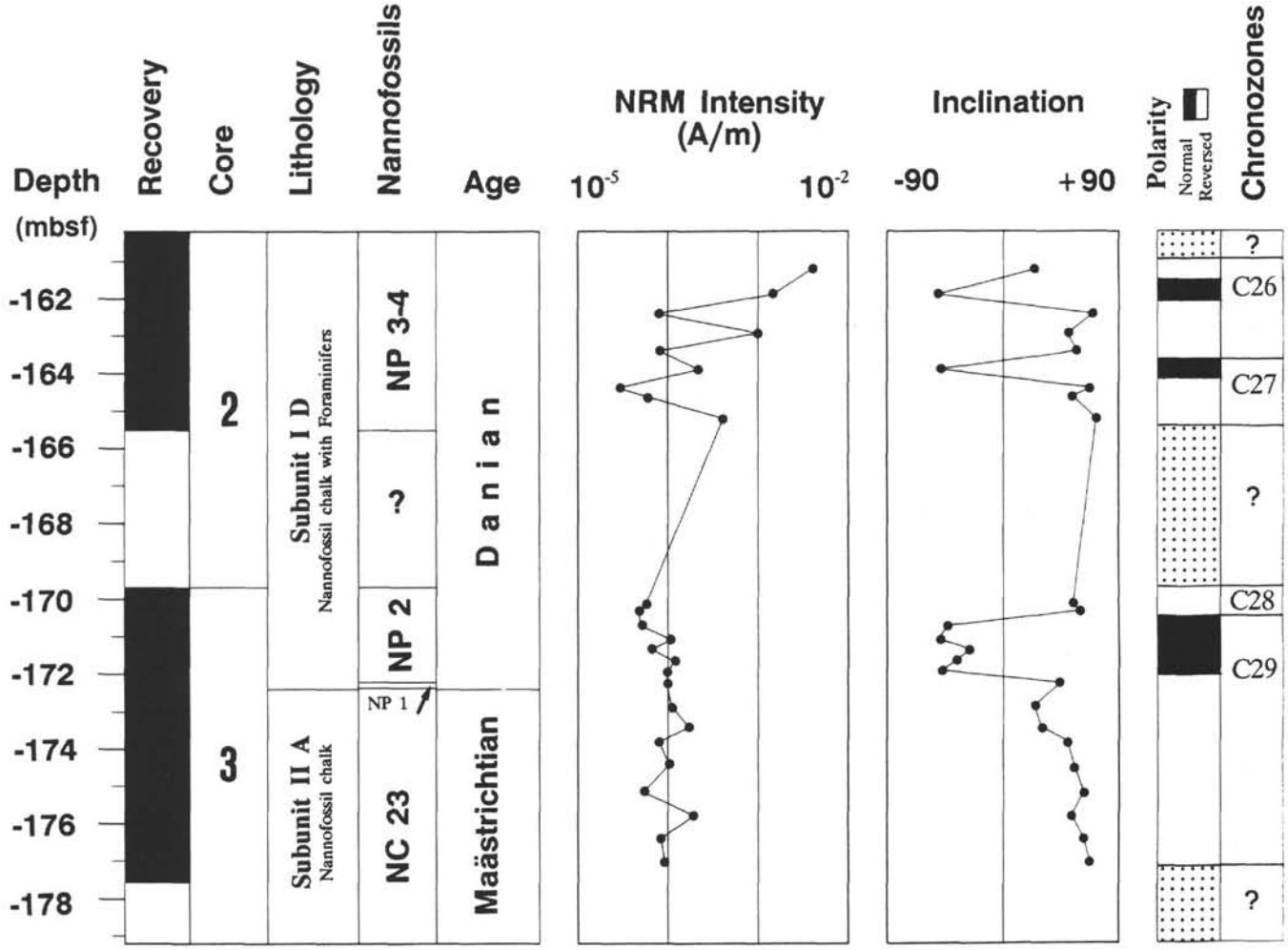

Figure 7. Maestrichtian/Danian boundary magnetostratigraphy of Hole 761C.

Table 3. Magnetostratigraphy and sedimentation parameters.

Position (mbsf)	Extent of Chron 29		
	Bottom of Chron 29R >177.05	K/T Boundary 172.47	Top of Chron 29N 170.33–170.72
Sedimentation parameters		Maestrichtian	Danian
Thickness of Chron 29 (m)		>4.58	1.75 to 2.14
Sedimentation rate (m/m.y.)		>10.4	1.1 to 1.3
Insoluble fraction (%)		≈9	≈30
Density (g/cm^3)		1.45	1.3
Mass accumulation rate (g/cm^2/1000 yr)		>1.51	0.14 to 0.17
Carbonate accumulation rate (g/cm^2/1000 yr)		>1.37	0.1 to 0.12
Insoluble fraction accumulation rate (g/cm^2/1000 yr)		>0.14	0.043 to 0.051

Can we conclude that all the observations at Hole 761C support the hypothesis of a comet or asteroid impact? Such events should have produced a considerable amount of ejecta, 10 to 100 times the mass of the impactor according to collisional models (O'Keefe and Ahrens, 1982). In Hole 761C this ejecta does not appear. The lack of a boundary clay layer, the constant mineralogical composition across the boundary, and the absence of chemical anomalies other than those of meteoritic elements suggest that the amount of ejecta is likely lower than one impactor mass. The slight change of the La/Yb ratio is probably not produced by an exotic component because the maximum occurs above the K/T boundary. It might be related to the drastic reduction of the carbonate productivity.

In short, it seems that the 0.16 g/cm^2 of Cl-like chondritic material derived from the Ir flux at Hole 761C were accreted in a pure state without mixing with an exotic terrestrial component. This observation is not unique; Jin and Schmitt (1989), using elemental results they obtained at Holes 577 and 577B (DSDP Leg 86) and by Michel et al. (1985) at Hole 577B in the central Pacific, estimated that the ejecta was less than half the impactor mass. The study of European sections leads to a similar conclusion (Rocchia et al., 1990). This can be explained in several ways: (1) a single impact did occur, but unlike extraterrestrial material, the ejecta was not evenly distributed over the Earth; or, more likely, (2) a significant fraction of the cosmic material was captured by the Earth as multiple small-sized fragments (fragmented comet, as already suggested by Kyte and Wasson (1982) and Schmitt (1989)), dispersing most of their mass in the atmosphere. Only the larger fragments would have produced craters and local deposits of ejecta, including shocked quartz. Apparently, K/T sediments at Holes 761C and 577 were not deposited close to a crater site.

CONCLUSION

Data from the K/T boundary at Hole 761C confirm the worldwide character of the Ir anomaly. The continuity of Ir distribution and the value of the Ir integrated flux (80 ng/cm^2, comparable with the K/T global average) show that the section is probably complete. In addition to Ir, enrichments in meteoritic elements (Cr, Fe, Co, Ni) are observed in close coincidence with a reduction of the sedimentation rate. Abundant Ni-rich magnetites of cosmic origin are also present in the basal Danian. This collection of data indicates a cosmic origin of the boundary event which, according to the Ir flux, resulted in the accretion of 0.16 g/cm^2 of Cl-like chondritic material. However, the accretion process is unclear. The extent of the Ir anomaly is not necessarily due to a long-duration event. On the other hand, the absence of any identifiable ejecta is not easily explained by a single impact. Other scenarios involving multiple small bodies losing and dispersing most of their mass in the atmosphere should be considered.

ACKNOWLEDGMENTS

The authors would like to thank the Ocean Drilling Program staff for preparing an exceptional set of samples. They are grateful to C. Pillmore and R. A. Schmitt for reviewing and improving this manuscript. This is CFR contribution no. 1117 and CNRS INSU-DBT contribution no. 224.

REFERENCES

Alvarez, L. W., Alvarez, W., Asaro, F., and Michel, H. V., 1980. Extraterrestrial cause for the Cretaceous-Tertiary extinction. *Science,* 208:1095–1108.

Bonté, P., Jéhanno, C., Maurette, M., Brownlee, D. E., 1987. Platinum metals and microstructure in magnetic deep sea cosmic spherules. *Proc. Lunar Planet. Sci. Conf. 17th, J. Geophys. Res.,* 92:E641–E648.

Brownlee, D. E., 1981. Extraterrestrial components in deep sea sediments. *In* Emiliani C. (Ed.), *The Sea:* New York (Wiley), 733–762.

Courtillot, V., and Cisowski, S., 1987. The Cretaceous-Tertiary boundary events: external or internal causes? *Eos,* 68:193–200.

Haq, B. U., Hardenbol, J., and Vail, P. R., 1987. Chronology of fluctuating sea levels since the Triassic. *Science,* 235:1156–1167.

_____, 1988. Mesozoic and Cenozoic chronostratigraphy and cycles of sea-level change. *In* Wilgus, C., et al., (Eds.), *Sea-Level Change–An Integrated Approach.* Soc. Econ. Paleontol. Mineral. Spec. Publ., 42:71–108.

Hut P., Alvarez, W., Elder, W. P., Hansen, T., Kauffman, E. G., Keller, G., Shoemaker, E. M., and Weissman P. R., 1987. Comet showers as a cause of mass extinctions. *Nature,* 329:118–126.

Jéhanno, C., Boclet, D., Bonté, P., Castellarin, A., Rocchia, R., 1987. Identification of two populations of extraterrestrial particles in a Jurassic hardground of the Southern Alps. *Proc. 18th Lunar Planet Sci. Conf.,* 623–630.

Jin, G.-Y., and Schmitt, R. A., 1989a. Pristine Shatsky Rise K/T marine carbonates yield Fe_{NET}/Ir_{NET} = C1 chondritic ratio: no evidence for Fe from terrestrial crater ejecta rules out direct asteroid-comet impact. I. Observations. *Lunar Planet. Sci. Conf. 20th,* 20:460–465. (Abstract)

Keller, G., 1989. Extended K/T boundary extinctions across the Cretaceous/Tertiary boundary in planktonic foraminifera of continental-shelf sections: implications for impact and volcanism theories. *Geol. Soc. Am. Bull.,* 101:1408–1419.

Kirschvink, J. L., 1980. The least-squares line and plane and analysis of paleomagnetic data. *Geophys. J. R. Astron. Soc.,* 62:699–718.

Kyte, F. T., and Smit, J., 1986. Regional variations in spinel compositions: an important key to the Cretaceous/Tertiary event. *Geology,* 14:485–487.

Kyte, F. T., and Wasson, J. T., 1982. Geochemical constraints on the nature of large accretionary events. *Spec. Pap. Geol. Soc. Am.,* 190:235–242.

_____, 1986. Accretion rate of extraterrestrial matter: iridium deposited 33 to 67 million years ago. *Science,* 232:1225–1230.

Michel, H. V., Asaro, F., Alvarez, W., and Alvarez, L. W., 1985. Elemental profile of iridium and other elements near the Cretaceous-Tertiary boundary in Hole 577B. *In* Heath, G. R., Burckle, L. H., et al., *Init. Repts. DSDP,* 86: Washington (U.S. Govt. Printing Office), 533–538.

Montanari, A., Hay, R. L., Alvarez, W., Alvarez, L. W., Asaro, F., Michel, H. V., and Smit, J., 1983. Spheroids at the Cretaceous/Tertiary boundary are altered impact droplets of basaltic composition. *Geology,* 11:668–671.

Officer, C. B., and Drake, C. L., 1983. The Cretaceous-Tertiary Transition. *Science,* 219:1383–1390.

_____, 1985. Terminal Cretaceous environmental events. *Science,* 227:1161–1167.

O'Keefe, J. D., and Ahrens, T. J., 1982. The interaction of the Cretaceous-Tertiary extinction bolide with the atmosphere, ocean, and solid Earth. *Spec. Pap. Geol. Soc. Am.,* 190:103–120.

Robin, E., Christophe Michel-Levy, N., Bourot-Denise, M., and Jéhanno, C., 1990. Crystalline micrometeorites from Greenland blue lakes: their chemical composition, mineralogy and possible origin. *Earth Planet. Sci. Lett.,* 97:162–176.

Rocchia, R., Boclet, D., Bonté, P., Devineau, J., Jéhanno C., and Renard, M., 1987. Comparaison des distributions de l'iridium observées à la limite Crétacé-Tertiaire dans divers sites européens. *Mem. Soc. Geol. Fr.,* N.S., 150:95–103.

Rocchia, R., Granier, B., Bellier, J.-P., Boclet, D., Bonté, P., Fourcade, E., Galbrun, B., Jéhanno, C., Lambert, B., Rasplus, L., and Renard, M., 1990. La limite Crétacé-Tertiaire du site de Finestrat (Province d'Alicante, Espagne). *C. R. Acad. Sci. Ser. 2,* 310:391–397.

Schmitt, R. A., 1989. Cometesimal explosions in Earth's atmosphere and steep angle cometesimal cratering events cause Cretaceous-Tertiary extinction phenomena. *Lunar Planet. Sci. Conf. 20th,* 962–963. (Abstracts)

Shipboard Scientific Party, 1990. Site 761. *In* Haq, B. U., von Rad, U., O'Connell, S., et al., *Proc. ODP, Init. Repts.,* 122: College Station, TX (Ocean Drilling Program), 161–211.

Smit, J., and Kyte, F. T., 1984. Siderophile-rich magnetic spheroids from the Cretaceous-Tertiary boundary in Umbria, Italy. *Nature,* 310:403–405.

Smit, J., and Romein, A.J.T., 1985. A sequence of events across the Cretaceous-Tertiary boundary. *Earth Planet. Sci. Lett.,* 74:155–170.

Timothy, D. H., and D'Hondt, S. L., 1990. Precessional climate cyclicity in Late Cretaceous–Early Tertiary marine sediments: a high resolution chronometer of Cretaceous-Tertiary boundary events. *Earth Planet. Sci. Lett.,* 99:263–275.

Zachos, J. C., Arthur, M. A., Thunnell, R. C., Williams, D. F., Tappa, E. J., 1985. Stable isotope and trace element geochemistry of carbonate sediments across the Cretaceous/Tertiary boundary at Deep Sea Drilling Project Hole 577, Leg 86. *In* Heath, G. R., Burckle, L. H., et al., *Init. Repts. DSDP,* 86: Washington (U.S. Govt. Printing Office), 513–532.

Date of initial receipt: 30 April 1990
Date of acceptance: 15 January 1991
Ms 122B-179

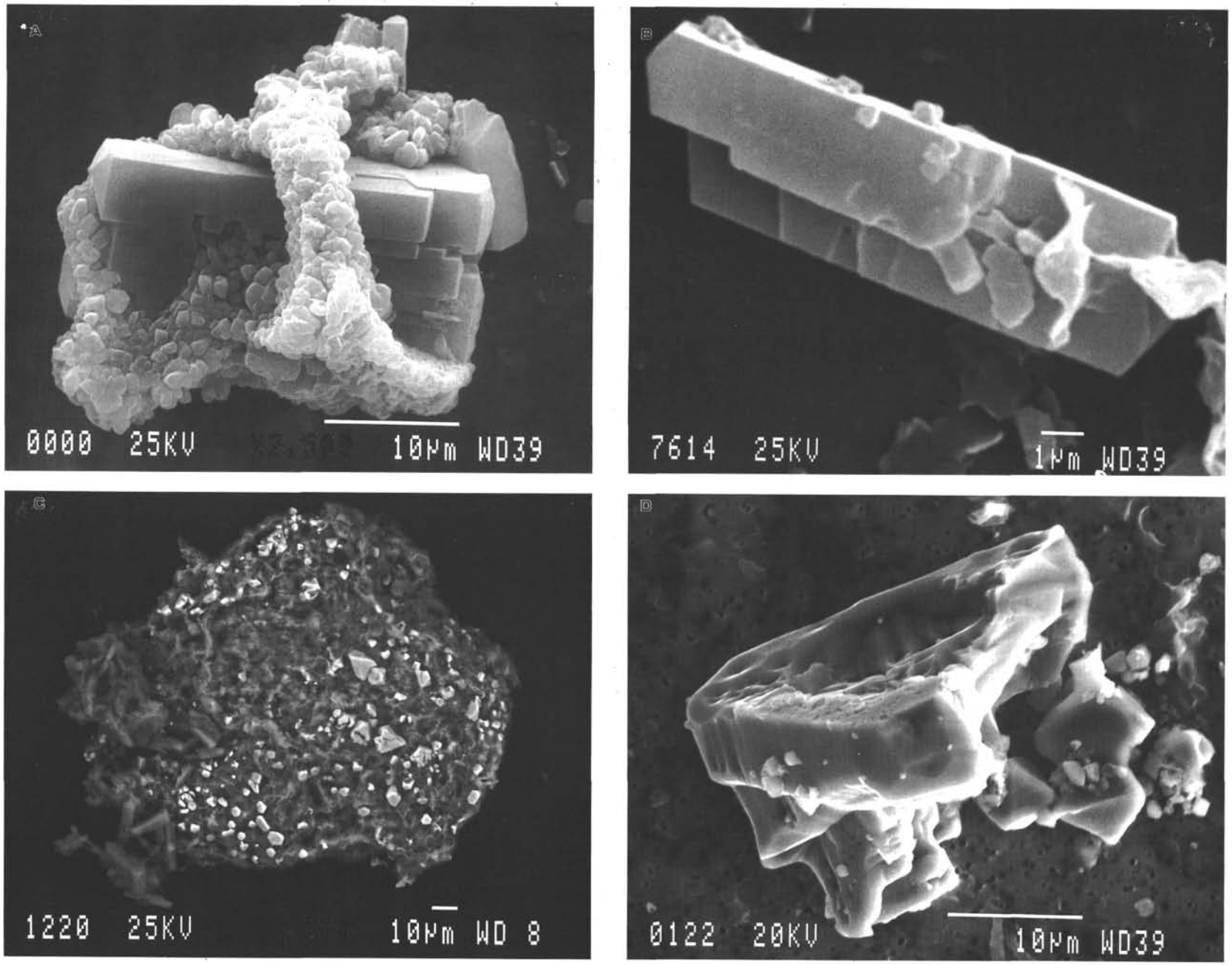

Plate 1. **A.** Clinoptilolite crystal that has grown inside a foraminifer test. **B.** Isolated clinoptilolite crystal. **C.** Magnetite-bearing flattened spheroid. Bright spots are magnetite crystals. **D.** Large Ni-rich magnetite.